Determination of dominant degradation mechanisms of RC bridge deck slabs under cyclic moving loads

Pengru Deng[1] and Takashi Matsumoto[2]

[1]Faculty of Engineering, Hokkaido University, Hokkaido 060-8628, Japan; Tel: +81-90-6213-5982; Email: dengpengru1989@gmail.com

[2]Faculty of Engineering, Hokkaido University, Hokkaido 060-8628, Japan; Tel: +81-11-706-6171; Email: takashim@eng.kokudai.ac.jp

ABSTRACT

In this paper, fatigue behaviors of RC bridge deck slabs which fail in an unexpected but widely observed punching shear failure mode under cyclic moving loads is analyzed following a fracture mechanics based theoretical method. This method is developed focusing on the propagation and failure along the critical punching shear cracks. From analysis, some key indicators of structural fatigue performances, including the fatigue crack growth of critical punching shear crack, stress evolutions of all materials and sectional forces, moments and crack mouth opening displacements (CMODs) due to all components along the critical punching shear crack cross sections and fatigue life, are obtained. These information are then based on to identify the dominant degradation mechanisms of RC bridge deck slabs subjected to cyclic loads, which provides meaningful and reliable references for the development of an efficient and accurate numerical method.

KEYWORDS

RC bridge slabs; Cyclic moving load; Crack bridging; Punching shear; Fatigue

1 INTRODUCTION

In the last few decades, due to an overlook of the shear capacity, especially fatigue shear capacity, of RC bridge deck slabs in previous design codes, a brittle and catastrophic punching shear failure mode is commonly observed in RC bridge deck slabs under service around the world as reported in [1-3]. To uncover the punching shear failure mode of RC bridge deck slabs, an amount of experimental works have been conducted systematically. In these experiments, a cyclic moving load was widely employed because both the punching shear failure mode and a shorten fatigue life of RC bridge deck slabs under service were successfully reproduced under this load condition as reported in [4-6]. However, as the experimental researches are always very costly and the design of an experimental set-up that can simulate load conditions approximate to the loads in reality is very complicated, the development of an accurate and efficient numerical method is required. In order to develop an efficient method for predicting fatigue performances of RC bridge deck slabs under cyclic moving loads, dominant degradation mechanisms should be identified beforehand and then included into the numerical method.

Zahran et. al. analyzed the fatigue strength of steel-concrete sandwich beams using the finite element method (FEM) in [7]. Tailored constitutive models were employed considering fatigue effects by reducing stiffness and strength of material models and the reductions were determined following some empirical formulations from experimental analysis. This investigation indicated that the effect of the reduction in compression stiffness is negligible. Regarding the bridging stress degradation of concrete as a primary degradation mechanism, fatigue behavior of RC bridge slabs subjected to cyclic moving loads were successfully predicted in [8-9]. These literatures concluded that the bond slip effect should be efficiently included for an accurate fatigue analysis. The characterized mode of failure under cyclic moving loads was reproduced based on a direct path-integral scheme with fatigue constitutive models of concrete as well in [10]. From the existing FEM based numerical analysis, it was concluded that fatigue modeling for concrete under tension and rebar/concrete interface bond slip play important roles in predicting the fatigue behavior of RC bridge slabs under cyclic moving load. However, in existing researches, the dominant degradation mechanisms were identified, employed and considered based on experiences from experimental analysis or numerical parametric studies. Thus, the employed dominant degradation mechanisms for accurately analyzing one case may be not applicable for another case because the dominant degradation mechanisms vary along with structural styles and failure modes.

In this study, an analytical method of determining the fatigue behavior of RC bridge slabs under cyclic moving loads is proposed focusing on the propagation of the punching shear cracks, where two generally accepted dominant degradation mechanisms, i.e. rebar/concrete bond slip degradation and concrete bridging degradation, are considered as the source of crack propagation. From this method, not only the fatigue life can be predicted but also the stress histories, i.e. stress levels, stress amplitudes and number of loading cycles, of all components along the punching shear crack cross sections can be determined in the entire life range. As the degradation of a material subjected to repeated loads is directly related to the experienced stress history, whether a degradation of a material under a stress state should be considered in fatigue analysis can be determined with the obtained stress history simultaneously. In addition, to figure out sectional resistances from different components, i.e. cracked concrete, uncracked concrete, bottom and upper rebars, forces, moments and crack mouth opening displacements (CMODs) due to these components are calculated and compared as well. With the obtained stress state of each material and sectional resistant contribution from sectional resistant contribution from each component, judgments on the dominant degradation mechanisms of RC bridge slabs subjected to cyclic moving loads are made easily and confidently. Furthermore, compared with the existing empirical equations from fitting experimental data schematically and the FEM based numerical methods, this method can not only accounting for the degradation mechanisms but also save a lot of computing time (1-2 hours/load which is a small percentage of that for numerical methods). This time-saving characteristic makes it extremely suitable for parametric studies and further design code improvements.

2 METHODS

To establish theories on the punching shear failure analysis of RC bridge slabs, many experimental works have been conducted employing a cyclic moving load experimental set-up. Under this loading condition, crack patterns, punching shear failure mode and observed shortened fatigue life of RC slabs in service were successfully reproduced. A typical failure crack pattern for an RC slab subjected to cyclic moving loads is shown as in **Figure 1**. From b-b cross section, a series of parallel cracks vertically with respect to the bottom surface of the RC slab can be observed at the failure moment. It is these cracks diminishing the shear force transferring capability of the RC slab along longitudinal direction. As a result, it is reasonable assuming that all the shear force due to the moving load is supported by a part between two parallel cracks when the load moves onto this part. And each of these parts is regarded as one RC beam in this study. From experimental observations, all these RC beams failure in a punching shear model. The black dash areas on the bottom view of the failed RC slab correspond to the punching shear cracks. In addition, among all these RC beams, the most dangerous one locates in the midspan. The punching shear cracks of this critical RC beam can be observed from a-a cross section. It is found that these punching shear cracks propagate along lines almost 45° with respect to the bottom surface and symmetrical with respect to the moving load.

According to the cracking process and failure crack pattern of RC slabs under cyclic moving loads, some empirical life prediction equations illustrating the relationships between load levels and number of loading cycles were formulated successfully using a punching shear capacity of a critical RC beam as a normalizing parameter in [11-12]. In these equations, the punching shear cracks were assumed along the 45° lines in experiments. Geometries of this critical RC beam and the 45° lines for punching shear crack paths are shown in **Figure 2**, where h and l are the depth and span of the RC beam, respectively; l_w and b are the length and width of the wheel/beam contact area; d_e is the effective depth for tensile rebar. In these empirical equations, the punching shear capacity of the critical beam is the only parameter used except for applied loads and number of loading cycles, which indicates that the fatigue life of the RC slab depends on the fatigue life of the critical RC beam.

Therefore, in this study, the life prediction of an RC bridge slab under a cyclic moving load is simplified into the life prediction of a critical RC beam and focused on the propagation of punching shear cracks according to the fundamental theories of existing researches and fatigue behavior of RC slabs under cyclic moving loads. The punching shear cracks are assumed to propagate along 45° lines symmetrical with respect to the moving load as shown in **Figure 2**.

For the critical RC beam subjected to general loads, sectional stresses acting on a cross section along the punching shear crack are shown in **Figure 3**, where no shear stress transferred in the cracked concrete is assumed because it is generally accepted that a cracking of RC members obeys the general law of fracture mechanics and should appear in a direction perpendicular to that of principal tensile stresses in the concrete. For every loading cycle, theoretically, the cracking states, such as crack depth and width, and the failure moment can be determined if all the sectional forces and stresses are available.

2.1 Basic assumptions

To determine these forces and stresses, firstly, three widely accepted assumptions are employed in this study as follows:

(1) Plane cross-section assumption: From this assumption, the strain distribution (ε_{II}) at the uncracked concrete and the normal strain of rebar on both compression (ε_{ru}) and tension zone (ε_{rb}) can be related to α and β as

$$\varepsilon_{II}(x)=\varepsilon_t\left(1-\frac{x-\alpha h}{\beta h-\alpha h}\right) \tag{1}$$

$$\varepsilon_{ru}=-\varepsilon_t\frac{h-(c+d_b/2)-\alpha h}{(\beta-\alpha)h} \tag{2}$$

$$\varepsilon_{rb}=\varepsilon_t\frac{h-(c+d_b/2)}{(\beta-\alpha)h} \tag{3}$$

where c is the cover depth. ε_t is cracking strain of concrete. α and β are crack depth and tensile depth ratios as shown in **Figure 3**.

(2) The cracked cross-section is assumed to rotate around the neutral axis. This assumption is also employed to study shear cracks of RC beams under four-point bending loads in [13]. From this assumption, the normal strain (ε_{rb}) and shear strain (γ_{rb}) for the longitudinal rebars at the crack location can be related with each other following the tensorial consideration. In addition, accounting for the relation between shear and normal elastic modulus for steel, one can obtain

$$V_{rb}=0.4T_{rb}\tan\varphi \tag{4}$$

where φ is the angle between crack and vertical direction as shown in **Figure 4**. This relation is valid as long as stresses in rebars are in the elastic phase, which can be ensured for RC beams or slabs failure due to shear.

(3) The crack has a linear crack opening profile as assumed in [14], then

$$w(x)=\delta\left(1-\frac{x}{\alpha h}\right) \tag{5}$$

where $w(x)$) is crack width at any location (x) along the crack. δ is crack mouth opening displacement (CMOD) as shown in **Figure 4**.

2.2 Formulate sectional forces and stresses with cracking state parameters

Using the materials strain and crack opening displacements from the section **2.1**, all the sectional stresses and forces are formulated as functions of cracking state parameters, i.e. α, β and δ, following appropriate material properties models.

(1) Sectional moment and shear force due to applied load

For a cracked RC slab under overall bending loads, the sectional stiffness is mainly from compressive concrete and tensile rebars, which stay in elastic range under service load conditions. Therefore, for the critical RC beam, the sectional moment due to applied load (M_A) can be formulated as a function of α through fitting results from finite element analysis (FEA) of the RC slab. However, as the RC slab is divided into some RC beams by a series of parallel cracks vertical to the moving load (**Figure 1**), shear forces cannot be transferred effectively to the adjacent beams when the load moves onto one beam, correspondingly the sectional shear force due to applied loads should be calculated through beam analysis. Thus, the shearing force (Q) for any cross section in the shear span is equivalent to half of the applied load.

(2) Stresses of uncracked concrete

From the assumed stress distribution, the stress for uncracked concrete, $\sigma_{II}(x)$, can be related to α and β as:

$$\sigma_{II}(x) = f_t\left(1 - \frac{x - \alpha h}{\beta h - \alpha h}\right) \tag{6}$$

where f_t is the tensile strength of concrete. No degradation is assumed for uncracked concrete under both tension and compression in this study.

(3) Stresses of cracked concrete

The stresses of cracked concrete are determined based on a crack bridging concept in [15-16]. In the first loading cycle, following a widely employed concrete bridging model illustrating the relationship between concrete bridging stress and crack width in [17], $\sigma_I(x)$ can be related to α and δ as

$$\sigma_I(x) = \frac{f_t}{1 + \left(\frac{\delta(1 - x/\alpha h)}{W_0} \right)^p} \tag{7}$$

where W_0 is the crack width corresponding to a reduction of the stress carrying capacity to 50% of the tensile strength. p is a shape factor. It has been reported that a concrete bridging model with p=1.2 and W_0=0.015mm fits a wide range of experimental data extremely well. These values are also used in this study.

From 2nd to Nth cycle, the concrete bridging stress is determined by replacing the concrete bridging model with a cycle dependent concrete bridging degradation model in [18-19]. Correspondingly, $\sigma_I(x)$ is related to α and δ as

$$\sigma_I(x) = \frac{f_t}{1 + \left(\frac{\delta(1 - x/\alpha h)}{W_0} \right)^p} \cdot [1 - d \log(N)] \tag{8}$$

where d is a stress degradation factor which can be related to the maximum crack width.

(4) Rebar stresses

In cracked RC structures, due to a rebar/concrete interface bond related tension stiffening effect, the rebar stress should vary along the rebar between cracks and peak at cracks. Therefore, generally there are two kinds of rebar stresses, i.e. average rebar stress and peak rebar stress at a crack.

In this study, the peak rebar stress at a crack is required, which is obtained through jointly employing a smeared crack model and a bond slip model. The smeared crack model is commonly employed in determining the average rebar stress. And the rebar stress distribution as well as the peak/average rebar stress relations can be determined following a bond slip model. Therefore, the peak rebar stresses at cracks can be determined with the obtained average rebar stresses from smeared crack model and peak/average rebar stresses relation from a bond-slip model.

The essential concept of smeared crack model for rebars is a space-averaged constitutive model accounting for bond slip effect. In this study, the space-averaged constitutive mode is obtained following a method introduced in [20], where the modified constitutive model was schematically shown in **Figure 5**. From this figure, it is found that there are two parameters, i.e. elastic modulus and yielding strength, should be modified to account for the bond effect. The modified yielding strength (f_y^*) and elastic modulus (E_s^*) are expressed as

$$\frac{f_y^*}{f_y} = \left(0.93 - 2Y\right) \tag{9}$$

and

$$E_s^* = \frac{f_y^*}{\varepsilon_s + \left(s_y / l_{tran}\right)} \tag{10}$$

where $Y = \left(f_t / f_y\right)^{1.5} / \rho$. ρ is the reinforcement ratio. ε_s is the strain of rebar corresponding to the stress of f_y^* in bare rebar model. s_y is the bond slip at f_y^*. l_{tran} is the transmission length which can be calculated following [21-23]. To account for the effect of the bond in the rebar/concrete interface on the modified constitutive model of rebars, bond slip models with or without degradation are employed in determining s_y.

In the first loading cycle, the relative slip at effective yielding stress (s_y) can be determined based on a local bond-slip-strain model in [24]. The model is expressed as

$$\frac{\tau}{f_c} = \frac{0.73\left(\ln\left(1 + 5s'\right)\right)^3}{1 + \varepsilon \times 10^5} \tag{11}$$

where ln is natural logarithm, ε is the local rebar strain, s' is the normalized slip equaling $1000S/d_b$, τ and S are local bond stress and local bond slip, respectively, f_c is concrete strength in MPa. The unit of slip (S) and rebar diameter (d_b) should be the same.

From 2nd to Nth cycle, a comprehensive local bond slip degradation model proposed by [25] is employed. This model was derived through statistically fitting results from experiments, where phenomenon reported in [26-27], such as cyclic increasing bond slip and no negative influence of cyclic loads on the bond strength, were found as well. The local bond slip degradation model is simply formulated with a cycle dependent slip (S_N), which can be expressed as a function of initial slip (S_1) by first cyclic loading and the number of cycles (N) as

$$S_N = S_1 N^m \tag{12}$$

The power m of **Eq. (12)** was found to be 0.098. Similar values for this power were reported according to test results, such as a 0.107 in [26].

So far, the modified rebar constitutive mode is obtained including the cyclic dependent bond slip condition. As the rebar strains from assumptions in section **2.1** can be treated as the averaged rebar strains, the averaged rebar normal stress is obtained through substituting this strain into the modified constitutive model and expressed as

$$\sigma_{sa} = E_s^* \cdot \varepsilon_t \frac{h - (c + d_b/2)}{(\beta - \alpha)h} \tag{13}$$

In addition, based on the bond-slip-strain model, the rebar strain distribution in a transmission length can be determined as well. Identifying to the average strain definition in [29] and the average strain concept in smeared crack model, the average rebar strain is calculated following the principle that the area under the average strain line is equivalent to the area under the strain distribution curve as illustrated in **Figure 6**. And then, the peak/average rebar strain is obtained and represented by a ratio as

$$e_s = \frac{\varepsilon_{s\max}}{\dfrac{\int_0^{l_{tran}} \varepsilon(t)dt}{l_{tran}}} \tag{14}$$

where $\varepsilon(z)$ is rebar strain at any point and t is the dummy variable for the integration. $\varepsilon_{\text{smax}}$ is the peak rebar strain at a crack. Correspondingly, the peak rebar normal stress at a crack is given as

$$\sigma_{rb} = e_s \cdot \sigma_{sa} \tag{15}$$

and the rebar shear stress can be determined following the relation illustrated in **Eq. (4)**. As a result, for every loading cycle, the rebar stresses at a crack are expressed by α and β based on a smeared crack model and a bond slip model.

In summary, except for the shear stress of uncracked concrete, all sectional stresses and forces are expressed with α, β and δ, which are named as cracking state parameters in this study. Mathematically, to determine α, β and δ after every loading cycle, at least three independent equations should be established with them.

2.3 Governing equations with cracking state parameters

As the shear stress distribution for a cracked cross section is not fully cognized so far, there are one force equilibrium equation along x direction and one moment equation can be established. These two equations are given as

$$\int_0^{\alpha h} \sigma_I(x)dx + \int_{\alpha h}^{h} \sigma_{II}(x)dx + T_{rb} + T_{ru} = 0 \tag{16}$$

$$\int_0^{\alpha h} \sigma_I(x)[(h-x)+(\alpha h - x)]dx + \int_{\alpha h}^{h} \sigma_{II}(x)(h-x)dx + T_{rb}\cdot(h-a_{sb}) + V_{rb}\cdot(\alpha h - a_{sb}) + T_{ru}\cdot a_{su} = M_A \tag{17}$$

where a_{sb} and a_{su} are the distance from rebar centroid to beam surface for bottom and upper rebars, respectively. M_A is sectional moment due to applied loads.

In order to obtain a complete solution, another equation is necessary. According to the cracking analysis of RC structures in [30], a CMOD decomposition equation can be established following an idea that the total CMOD is a summation of CMODs due to applied loads, crack bridging elements and rebar/concrete interface bond slip. This CMOD decomposition equation is expressed as

$$\delta = \delta_A(\alpha) + \delta_I(\sigma_I(x), \alpha) + \delta_{rb\&s}(T_{rb}, V_{rb}, \alpha) \tag{18}$$

where δ_A and δ_I are CMODs due to applied loads and concrete bridging stresses. $\delta_{rb\&s}$ is CMOD due to rebar bridging stresses and a rebar/concrete interface bond slip. Since the bond slip is included in the modified rebar stress-strain relation, CMODs due to rebar bridging stresses and the bond slip are calculated together. All the CMODs appeared in the right side of **Eq. (18)** can be calculated employing a fracture mechanics based integral equation introduced in [30-32]. In this integral equation, crack face weight functions are necessary for the crack geometries. As **Eq. (18)** is about crack mouth opening displacements, only Mode I weight function components are required. For an inclined edge shear crack in an RC beam, the crack face weight functions are obtainable based on a finite element method (FEM) based virtual crack extension technique introduced in [33].

With the established three governing equations from **Eq. (16)** to **(18)**, the cracking state parameters, i.e. α, β and δ, can be determined through solving the equations after every loading cycle. Moreover, all sectional stresses and forces are obtainable as well because they are functions of α, β and δ.

2.4 Failure moment determination with cracking state parameters

In this study, the final failure is determined through checking shear load capacities along the punching shear cracks in the critical RC beam according to the observed experimental failure crack pattern and existing theories. And the total shear resistance is considered as a summation of the shear strength of concrete and dowel actions of longitudinal rebars.

For the shear strength of concrete, under cyclic moving loads, the formed cracks experience repeated opening and closing process, which keep polishing the interface of aggregates and mortar. Consequently, the stress transferring capability of concrete reduces dramatically to almost zero at the failure moment, which means only uncracked concrete can provide shear resistance. In terms of the dowel action of longitudinal rebars, both upper and lower rebars should be included. However, post-moment inspections of tested specimens showed that a delamination at the upper rebars level occurred in the mid-span cross-section of specimens subjected to cyclic moving loads as shown in **Figure 7**. This is probably a result of high-fatigue shear stresses at that depth due to the existence of upper rebars and a short distance from the neutral axis. These lateral shear cracks and a related reduction of punching shear capacity were observed in pulsating fatigue specimens in [3], where both static and pulsating loads were employed. As a result, the dowel effect of upper rebars should not be included in determining the punching shear capacity after the crack tip reaches upper rebars.

Accounting for these considerations, the shear resistance from concrete and rebars are determined following AASHTO and ACI equations in [1, 34] for punching shear capacity and dowel strength equation in [11], respectively. Finally, the punching shear capacity of a critical RC beam is related to the cracking state parameters and given as

$$V_{pun} = \begin{cases} 2\left[b+(1-\alpha)h\right]\cdot(1-\alpha)h\cdot f_t + 4c\cdot B\cdot f_t & \text{Before crack tip reaching upper rebars} \\ 2\left[b+(1-\alpha)h\right]\cdot(1-\alpha)h\cdot f_t + 2c\cdot B\cdot f_t & \text{After crack tip reaching upper rebars} \end{cases} \quad (19)$$

The failure moment is determined based on this punching shear capacity in this study.

3 METHOD APPLICATION

In this study, a fatigue analysis based on the proposed method is conducted to investigate crack propagation, predict fatigue life and identify the dominant degradation mechanisms of RC bridge slabs under cyclic moving loads. To facilitate method verification, the method is applied to analyze an RC slab tested by the Civil Engineering Research Institution for Cold Region (CERI) [35]. The dimension of the tested slab is 2,650 × 3,300 × 160 mm with a cover depth 32 mm for both tensile and compressive rebars. Detail information of dimensions, boundary conditions, load conditions and reinforcement arrangement for the RC slab are shown in **Figure 8**. A cyclic wheel load moves on a loading plate supported by a series of isolated small plates with a size 200 × 500 mm which is identical to the contact area size of an actual wheel load. Properties of concrete and steel rebars are listed in **Table 1**. With these information, the critical RC beam corresponding to the RC slab can be determined as shown in **Figure 2**. In this study, a fatigue analysis of the RC slab is conducted on this RC beam and focused on a couple of 45° punching shear cracks symmetrical with respect to the moving load land.

3.1 Evolutions of cracking state parameters

In this study, four load levels from 130kN to 200kN, are selected for fatigue analysis. The crack depth/beam depth ratios at these loading levels are plotted with the number of loading cycles on the semi-logarithmic scale shown in **Figure 9(a)**. Generally, it is found that the theoretical simulation successfully captured the first two stages of general fatigue growth of a bridged crack in concrete structures, i.e. initial decelerated growth and steady state growth stages. The trends exhibited in these curves can be understood according to the relative relations between Mode I crack tip stress intensity factors (SIFs) due to applied loads and all bridging elements as interpreted in [15]. The reason why the final accelerated crack growth state cannot be observed is that the RC beam is assumed failing in a brittle shear failure mode according to certain failure criterion. Specifically, the initial decelerated stage in the crack depth/beam depth ratio to number of loading cycle curves for higher load levels is not as apparent as that for lower load levels. This is because the punching shear crack is more fully developed in the beginning loading cycles under the higher load levels, manifested with higher crack depths and wider crack openings. Due to the wide crack opening, the bridging effect from nonlinear concrete bridging stress maybe small or even negligible compared with that from rebars. As a result, the crack propagation curves seem to start from the steady state growth for higher load levels as observed in **Figure 9(a)**.

Similar to the characteristics exhibited in the crack depth/beam depth ratio to number of loading cycles relations, the initiate two crack growing stages are also observed in **Figure 9(b)**, where the relationships between tensile depth/beam depth ratio and the number of loading cycles for several fatigue loading levels are plotted on the semi-logarithmic scale.

The evolution of CMODs with respect to the increasing number of loading cycles for several fatigue loading levels are drawn on a semi-logarithmic scale as in **Figure 9(c)**. It is noticed that the CMOD evolution of the punching shear crack depends on the loading level. However, the two stages observed in **Figure 9(a)** and **Figure 9(b)** are not apparently exhibited. Especially for the second stage where a continuous increasing rather than a steady stable of CMOD is observed for all load levels. As the crack depth reaches a stable in the second stage, the CMOD due to applied load and crack bridging stress should stay almost unchanged. Thus, the CMOD increasing in the second stage is expected to be mainly from the degradation of bond slip.

3.2 Fatigue life prediction

With the obtained values for cracking state parameters after every loading cycle as shown in **Figure 9**, the punching shear capacity can be determined following **Eq. (19)**. And then, a judgment on whether the final failure occurs or not can be made through comparing the applied load and the determined punching shear capacity. For each load level, the determined failure moment is the fatigue life from the proposed method. In addition, the fatigue life can be calculated following some empirical life prediction equations in [5, 12] derived by different research groups, such as Matsui and Abe research teams, and institutions, such as Japan Society of Civil Engineers (JSCE) and Public Work Research Institute (PWRI). All these empirical equations were derived through statistically fitting a huge set of experimental results of RC slabs tested under a similar experimental set-up but with different material properties, reinforcement ratios and dimensions. Therefore, these equations implicitly reflect the internal mechanisms and can be employed in life prediction of similar problems as the employed case in this study.

The S-N diagrams of the proposed theoretical method and all empirical life prediction equations and experimental fatigue life in [35] are plotted on a double-logarithmic scale as shown in **Figure 11**, where the vertical and horizontal axes represent a load parameter normalized with a punching shear capacity determined by [5] and number of loading cycles, respectively. It is found that the theoretical S-N relation agrees well with the experimental fatigue life of the tested RC slab. In addition, the obtained S-N relation is approximately the average result of the four reported fatigue life prediction equations derived statistically. These good agreements verify the reliability of the proposed theoretical method.

3.3 Stress evolutions of different components

Figure 11(a) shows the relationship between rebar normal and shear stresses at cracks and the number of loading cycles. It is noticed that the rebar stress increases with the increasing number of cycles and approaches an asymptote-resembled line. The value of this line depends on the loading level and is much lower than the yielding strength of rebars even under a relatively high load level, 200kN. This means the Baushinger effect of tensioned rebar which consists of a reduction of yielding strength after a reverse and decrease of curvature in the transition zone between the elastic and plastic branches can be neglected. In addition, it is found that the rebar stress experienced a relative high speed of rising in the initial several loading cycles, especially for lower load levels. This can be explained as: under the initial narrow crack opening, the concrete bridging stress accounts for a large proportion of the total bridging effect. The stress transferring ability of cracked concrete decreases due to the damage caused by the crack opening and closing process, which is considered through introducing a concrete bridging degradation model. As a result, the forces which were supposed to be sustained by the cracked concrete were transferred to the rebars. With increasing number of cycles, the opening and closing processes keep smoothing both faces of the crack and finally the concrete bridging stress reduces to almost zero. Correspondingly, the rebar stresses reach a plateau state. The final asymptote-resembled rebar stress level can be regarded as the rebar stresses computed without accounting for the tensile effect of concrete. As shown in **Figure 9(a)** and **(b)**, the crack grows with a very slow speed in the steady state, which means the internal force lever between the stress resultant point of components in the compression zone and the bottom rebars stays almost unchanged. Thus, the rebar stress should remain almost constant under the same sectional moment from applied load as indicated in **Figure 11(a)**. The notable rebar stress increase is due to the concrete bridging stress degradation, which confirms the necessity of including concrete bridging degradation in the fatigue analysis of a RC slab subjected to cyclic moving load indirectly.

The variations of the maximum compression stress of concrete at several fatigue loading levels are plotted with the number of loading cycles on a semi-logarithmic scale as shown in **Figure 11(b)**. Even though the absolute values of maximum compression stress keep growing, the final values under all the selected loading levels are in a relatively low level, less than 30% of compression strength. Under this stress level, the fatigue life of concrete can be up to 10^{12} loading cycles following the S-N relationship presented in [36]. This fatigue life is much longer than the ACI provisions employed threshold value for fatigue life, ten million cycles, which means the degradation of concrete in the compression zone is negligible. The degradation of concrete was also reported as negligible if the maximum stress is lower than 30% of compression strength in [37], where a versatile model on analyzing the fatigue degradation of compressed concrete was proposed through introducing a low cycle concept. All these results indicate that the degradation of concrete in the compression zone is negligible for an accurate fatigue analysis of an RC slab under cyclic moving load.

3.4 Contributions from different components

For the punching shear crack in the critical RC beam under applied loads, the sectional rotation and crack opening are resisted by stresses from all components, i.e. bottom rebars, cracked concrete, uncracked concrete and upper rebars. There should be some components playing dominant roles in balancing the applied load. These components can be identified if contributions from all components are computed. On the basis of the contributions from all components in the whole life, a more straight-forward and confident image on the fatigue behavior of RC slabs under cyclic moving load can be figured out. Furthermore, the determined dominant components provide advice and references to researchers who are purposed at developing simulation methods as efficient as possible.

In this section, for several loading levels, the forces, moments and CMODs due to different components in the cross-section along the punching shear crack are computed after certain number of cycles using the obtained three cracking state parameters. Since a two-dimensional crack model is assumed for the cracked RC beam, all the forces and moments given in this sections are the forces and moments acting on unit width of the beam. Based on the obtained results, some discussions on the dominant sectional rotation and crack opening resistant components are given, respectively.

3.4.1 Forces from different components

For a selected cross-section, the forces from all components make up a self-equilibrium system. According to the force acting direction, the components can be roughly divided into two groups, i.e. bottom rebars and cracked concrete, uncracked concrete and upper rebars.

The relationships between forces from bottom rebars and number of loading cycles for several loading levels are shown in **Figure 12(a)**, where the curve trends are exactly the same as the trends observed in the bottom rebar stress curves (**Figure 11(a)**). This is because the forces of the bottom rebars can be related to the corresponding stresses with a constant rebar area.

Figure 12(b) shows the relationship between forces from cracked concrete and number of loading cycles for several loading levels. For each curve, the forces decline rapidly to a small amplitude and then reach a steady state, which means the concrete bridging stress degradation occurs quickly after the initiation of a crack. This is why the fatigue life of a plain concrete structure is much shorter than a reinforced concrete structures as reported in [14]. From the four curves, it is found that, due to the wider crack opening under a higher load level, the forces from cracked concrete decrease with the increasing applied load level. If **Figure 12(b)** is investigated jointly with **Figure 12(a)**, the relative relationships between forces between bottom rebars and cracked concrete are obtainable. **Figure 12(a)** and **(b)** indicate that the forces of bottom rebars are generally larger compared to the forces for cracked concrete, and that the different between them becomes larger as the increasing number of loading cycles. Under all load levels, the forces from cracked concrete decline to almost negligible compared with the bottom rebar forces before final failure.

Figure 12(c) and **(d)** show the variations the forces from uncracked concrete and upper rebars, which are mostly in the compression zone, after each number of loading cycles in semi-logarithmic scales, respectively. It is seen from **Figure 12(c)** that the forces from uncracked concrete depend on the load level and, except for curve for 130kN, the forces from uncracked concrete remain almost unchanged in other cases. This is because, as shown in **Figure 9**, only the punching shear crack under 130kN loading condition experienced a remarkable uplifting of tensile depth/beam depth ratio, which reflects the internal force lever between compressed and tensioned components. In terms of the forces from upper rebars as shown in **Figure 12(d)**, the absolute values of these forces are much lower than those from the other components. In addition, due to the continuous growing tensile depth, the sectional neutral axis may surpass the center point of upper rebars and correspondingly the stress state of upper rebars is transformed from compression into tension as indicated in **Figure 12(c)**.

Figure 13 compares the forces from different components versus number of loading cycles for applied load ranging from 130kN to 200kN. The variations of relative magnitude relationships among all the components over load levels and number of cycles can be more easily visible from **Figure 13**. It is found that the magnitude of force from upper rebars is always much smaller than that from other components, which means the effect of upper rebars on resisting sectional rotation can be simply neglected conducting calculation. For the contribution from the cracked concrete which is generally regarded as zero in sectional analysis of RC beams, even though the magnitude decrease with the increasing load level, it cannot be neglected for structural analysis of RC slabs under service loading levels compared with the contribution from bottom rebars. However, as is assumed in design codes, the bridging effect of concrete can be ignored for determining both static and fatigue ultimate load capacity.

3.4.2 Moments from different components

Considering the variation of height of sectional neutral axis for different load levels and number of cycles, the moments from all components are computed with respect to the upper surface of the beam and given in this section. For the moments from both bottom and upper rebars shown in **Figure 14(a)** and **Figure 14(d)**, the curves exhibit the same trends as observed in the corresponding forces owing to the constant force levers for all rebars.

In the semi-logarithmic scale, **Figure 14(b)** shows the variations of moments from cracked concrete with the increasing number of loading cycles for several load levels. As the reduction of moment from cracked concrete is a result of the combined action of reductions of both cracked concrete forces and forces levers, the moments from cracked concrete drop at a higher speed compared with the trends of cracked concrete forces as indicated in **Figure 12(b)**.

The relationships between moment from uncracked concrete and number of loading cycles are plotted in a semi-logarithmic scale for several loading levels as shown in **Figure 14(c)**. It is found that the curve for 130kN can be divided into two stages: decelerated decrease stage, stable stage. The two stages can be explained as follows. Generally, the stress distribution of uncracked concrete can be shown as in **Figure 15**. With respect to top point of the cross-section, moments from uncracked concrete above and below the neutral axis are in opposite signs. As illustrated in **Figure 12(c)**, the forces from uncracked concrete are with a negative sign in all situations, which means the absolute value of the resultant force from uncracked concrete below the neutral axis. However, the force lever for the uncracked concrete below the neutral axis is larger than that of above the neutral axis. If the distance from the neutral axis to the top point is smaller than 2 times of the distance from the crack tip to the neutral axis, the moment from uncracked concrete should be in a positive sign as observed in the beginning several cycles of the curve for 130kN. Owing to crack growing, the crack tip approaches to the neutral axis, and the moment from uncracked concrete below the neutral axis decreases rapidly. As a result, the decelerated decrease stage is observed in the curve for 130kN. This decrease stops when the crack growth reaches the steady stable stage, and the moment from uncracked concrete enters the stable stage as well. According to the interpretation of the curve for 130kN, the range and presence of decelerated decrease stage depend on the extent of crack propagation in the initial number of cycles. Since the crack becomes more developed after several initial loading cycles for high loading levels, the range of the decelerated decrease stage shortens and then even disappears with the increasing loading levels as shown in **Figure 14(c)**.

3.4.3 CMODs from different components

As illustrated in section **2.3**, the crack opening is a result of combined action of applied loads, rebar forces, bond slip and concrete bridging stresses. However, through employing the modified rebar constitutive model, the crack opening due to bond slip is included in the crack opening due to rebar forces. Therefore, only the evolutions of three CMODs, i.e. CMOD due to applied load, CMOD due to rebar forces and CMOD due to concrete bridging stresses, are presented in this section.

The evolutions of CMODs due to rebar forces with the increasing number of loading cycles are drawn in **Figure 16(a)** for several loading levels. The trend of these curves maybe difficult to be understood theoretically because the CMODs due to rebar forces are calculated following the complicated energy based integral equation as introduced in [30-32]. However, these curves are easily understandable from the physical meaning of crack opening. For an existing crack, the crack faces can be regarded as a cantilever beams rotating around the crack-tip. Thus, the rebar force lever increases with the propagation of the crack. At the same time, the magnitude of rebar forces increases as well. Therefore, the growing speed of the magnitude of CMOD due to rebar forces is a summation of growing speed of crack propagation in **Figure 9** and rebar force increasing shown in **Figure 11**.

The relationships between CMODs due to cracked concrete and number of loading cycles for several loading levels are shown in **Figure 16(b)**, where the characteristics of all curves can be explained similarly as the explanation for the CMODs due to rebar forces. The resultant forces of cracked concrete decrease with the increasing number of cycles; meanwhile, the resultant force points approach the crack-tip because the concrete bridging stress degrades more dramatically for locations close to the crack mouth. Consequently, CMOD due to cracked concrete drops to a very low magnitude rapidly as shown in **Figure 16(b)**.

Figure 16 presents the variations of CMODs from different components versus number of loading cycles in semi-logarithmic scales for several loading levels. It can be found that, except for the initial certain number of loading cycles under 130kN, the crack bridging effect is mainly from the rebars. Therefore, to calculate the width of a crack in degraded RC structures or RC structures under relatively high loading levels, the crack bridging effect of concrete can be simply regarded as negligible. This is why many researches on determination of crack widths of RC structures can achieve an acceptable accuracy without considering the effect of concrete bridging stress.

4 CONCLUSIONS

Based on nonlinear fracture mechanics of RC structures, a fatigue analysis method for RC bridge deck slabs failed in a punching shear failure mode under cyclic moving loads was proposed focusing on the propagation and failure along the critical punching shear cracks.

In this method, the crack propagation was considered as a combined result of a concrete bridging stress degradation and a rebar/concrete interface bond slip degradation and the final failure was predicted following certain punching shear failure criterion using the obtained cracking states after every loading cycle. Specific findings and conclusions are summarized as follows:

Firstly, the developed method was applied into fatigue analysis of a tested RC slab under several service level resembled loads, where the fatigue crack growth of the critical punching shear cracks were predicted and then used to predict fatigue life following the punching shear failure criterion. Comparisons between method life predictions to results from experiment and some existing life prediction equations indicated a reasonably good agreement, which verified the applicability and reliability of the proposed method.

Moreover, stresses of bottom rebars and compressed concrete were calculated after every loading cycle as well. It was found that, under the selected loads, the rebar stresses and the maximum compression stresses of concrete were lower than the yielding strength of steel rebars and 30% of compression strength of concrete, respectively, in the whole life range, which means the degradations of tensioned rebars and compressed concrete are negligible for an accurate fatigue analysis of an RC slab under cyclic moving loads.

Furthermore, to identify dominant components resisting sectional rotation and crack opening, this method was also employed to compute forces, moments and CMODs from all components. The obtained results indicated that the bottom rebars and uncracked concrete play dominant roles in resisting sectional rotation and crack opening. However, the contribution from cracked concrete which is generally regarded as zero in sectional analysis of RC beams should be carefully considered, especially for fatigue analysis of RC beams under service loading conditions.

Conclusively, the presented study provided a theoretical method for understanding the fatigue behavior of RC bridge deck slabs under cyclic loads. In addition, it afforded some straight-forward and trustworthy references on the degradation mechanisms that should be included for the development of an accurate and efficient numerical method.

ACKNOWLEGEMENT

We are grateful to Dr. K. Kakuma from Civil Engineering Research Institute for Cold Region for providing us helpful suggestions and experimental data.

REFERENCES

[1] AASHTO, T. (1983). 277-83. Standard method of test for rapid determination of the chloride permeability of concrete, American Association of State Highway and Transportation Officials, Washington, DC.

[2] Schläfli, M., & Brühwiler, E. (1998). Fatigue of existing reinforced concrete bridge deck slabs. Engineering Structures, 20(11), 991-998.

[3] Graddy, J. C., Kim, J., Whitt, J. H., Burns, N. H., & Klingner, R. E. (2002). Punching-shear behavior of bridge decks under fatigue loading. ACI Structural Journal, 99(3).

[4] Perdikaris, P. C., & Beim, S. (1988). RC bridge decks under pulsating and moving load. Journal of structural engineering, 114(3), 591-607.

[5] Maeda, Y., & Matsui, S. (1984). Punching shear load equation of reinforced concrete slabs. Doboku Gakkai Ronbunshu, 1984(348), 133-141.

[6] Pedikaris, P., Beim, S., & Bousias, S. (1989). Slab continuity effect on ultimate and fatigue strength of reinforced concrete bridge deck models. Structural Journal, 86(4), 483-491.

[7] Zahran, M., Ueda, T., & Kakuta, Y. (1998). Shear-fatigue behavior of steel-concrete sandwich beams with shear reinforcement. Doboku Gakkai Ronbunshu, 1998(585), 217-231.

[8] Drar, A. A. M., & Matsumoto, T. (2016). Fatigue Analysis of RC Slabs Reinforced with Plain Bars Based on the Bridging Stress Degradation Concept. Journal of Advanced Concrete Technology, 14(1), 21-34.

[9] Suthiwarapirak, P., & Matsumoto, T. (2006). Fatigue analysis of RC slabs and repaired RC slabs based on crack bridging degradation concept. Journal of structural engineering, 132(6), 939-948.

[10] Maekawa, K., Toongoenthong, K., Gebreyouhannes, E., & Kishi, T. (2006). Direct path-integral scheme for fatigue simulation of reinforced concrete in shear. Journal of Advanced Concrete Technology, 4(1), 159-177.

[11] Matsui, S. (1987). Fatigue strength of RC-slabs of highway bridge by wheel running machine and influence of water on fatigue. Proceedings of JCI, 9(2), 627-632.

[12] Abe, T. (2015). Fatigue prediction life and evaluation of the integrity of road bridge RC slabs. Journal of Structural Engineering A, 61, 1050-1061.

[13] Zararis, P. D., & Papadakis, G. C. (2001). Diagonal shear failure and size effect in RC beams without web reinforcement. Journal of structural engineering, 127(7), 733-742.

[14] Zhang, J., Stang, H., & Li, V. C. (1999). Fatigue life prediction of fiber reinforced concrete under flexural load. International Journal of Fatigue, 21(10), 1033-1049.

[15] Li, V. C., & Matsumoto, T. (1998). Fatigue crack growth analysis of fiber reinforced concrete with effect of interfacial bond degradation. Cement and Concrete Composites, 20(5), 339-351.

[16] Matsumoto, T., & Li, V. C. (1999). Fatigue life analysis of fiber reinforced concrete with a fracture mechanics based model. Cement and Concrete Composites, 21(4), 249-261.

[17] Stang, H., Li, V. C., & Krenchel, H. (1995). Design and structural applications of stress-crack width relations in fibre reinforced concrete. Materials and structures, 28(4), 210-219.

[18] Hordijk, D. A. (1992). Tensile and tensile fatigue behaviour of concrete; experiments, modelling and analyses. Heron, 37(1).

[19] Zhang, J., Stang, H., & Li, V. C. (2001). Crack bridging model for fibre reinforced concrete under fatigue tension. International Journal of Fatigue, 23(8), 655-670.

[20] Dehestani, M., & Mousavi, S. (2015). Modified steel bar model incorporating bond-slip effects for embedded element method. Construction and Building Materials, 81, 284-290.

[21] CEB-FIP, C. (1991). model code 1990. Comite Euro-International Du Beton, Paris, 87-109.

[22] Eurocode 2 (1991. Design of concrete structures: part 1: general rules and rules for buildings. European Committee for Standardization.

[23] Borosnyói, A., & Balázs, G. (2005). Models for flexural cracking in concrete: the state of the art. Structural Concrete, 6(2), 53-62.

[24] Maekawa, K., Okamura, H., & Pimanmas, A. (2003). Non-linear mechanics of reinforced concrete: CRC Press.

[25] Oh, B. H., & Kim, S. H. (2007). Realistic models for local bond stress-slip of reinforced concrete under repeated loading. Journal of structural engineering, 133(2), 216-224.

[26] Rehm, G., & Eligehausen, R. (1979). Bond of ribbed bars under high cycle repeated loads. Paper presented at the ACI Journal Proceedings.

[27] Balázs, G., & Koch, R. (1992). Influence of load history on bond behaviour. Proceedings of the bond in concrete–from research to practice, October, Riga, Latvia, 7.1-10.

[28] Balázs, G., Koch, R., & Harre, W. (1994). Verbund von stahl in beton unter betriebsbeanspruchung. Deutscher ausschuss fr stahlbeton-30, Forschungskolloquium. Sttutgart, 1567-1590.

[29] Belarbi, A., & Hsu, T. T. (1994). Constitutive laws of concrete in tension and reinforcing bars stiffened by concrete. Structural Journal, 91(4), 465-474.

[30] Deng, P., & Matsumoto, T. (2017a). Estimation of the rebar force in RC members from the analysis of the crack Mouth opening displacement based on fracture mechanics. Journal of Advanced Concrete Technology, 15(2), 81-93.

[31] Nazmul, I., & Matsumoto, T. (2008a). High resolution COD image analysis for health monitoring of reinforced concrete structures through inverse analysis. International journal of solids and structures, 45(1), 159-174.

[32] Nazmul, I., & Matsumoto, T. (2008b). Regularization of inverse problems in reinforced concrete fracture. Journal of Engineering Mechanics, 134(10), 811-819.

[33] Deng, P., & Matsumoto, T. (2017b). Weight function determinations for shear cracks in reinforced concrete beams based on finite element method. Engineering Fracture Mechanics, 177, 61-78.

[34] ACI, B. (1999). 318-Building Code requirements for reinforced concrete and commentary. American Concrete Institute International.

[35] Mitamura, H., Satou, T., Honda, K., & Matsui, S. (2009). Influence of frost damage on fatigue failure of RC deck slabs on road bridge. Journal of Structural Engineering A, 55, 1420-1431.

[36] Kim, J.-K., & Kim, Y.-Y. (1996). Experimental study of the fatigue behavior of high strength concrete. Cement and concrete research, 26(10), 1513-1523.

[37] Zanuy, C., de la Fuente, P., & Albajar, L. (2007). Effect of fatigue degradation of the compression zone of concrete in reinforced concrete sections. Engineering Structures, 29(11), 2908-2920.

FIGURE LEGENDS

Figure 1 A typical failure crack pattern of an RC slab under cyclic moving loads

Figure 2 Geometry of the simplified RC beam and the punching shear cracks

Figure 3 Sectional stresses and forces

Figure 4 Schematic diagrams for basic assumptions

Figure 5 Modified stress-strain relationship for rebars embedded in concrete

Figure 6 Relation between peak rebar strain and average rebar strain

Figure 7 Experimental mid-span crack pattern of several RC slabs provided by Dr. K. Kakuma from CERI

Figure 8 RC slab geometry and reinforcement arrangement [35]

Figure 9 Cracking state parameters vs. number of loading cycles

Figure 10 Comparison between fatigue life from different approaches

Figure 11 Stress evolutions of materials

Figure 12 Forces from different components vs. number of loading cycles for several loading levels

Figure 13 Comparison of forces from different components vs. number of loading cycles for several loading levels

Figure 14 Moments from different components vs. number of loading cycles for several loading levels

Figure 15 Stress distribution in the uncracked concrete

Figure 16 CMODs due to different components vs. number of loading cycles for several loading levels

TABLES

Table 1 Material properties

Materials	Properties	Values (MPa)
Concrete	Compression strength (f_c)	43.2
	Tensile strength (f_t)	2.88
	Shear strength (f_v)	5.66
	Elastic modulus (E_c)	25,442
Steel rebar (SR235)	Yielding strength (f_y)	341
	Tensile strength	462
	Elastic modulus (E_s)	200,000

FIGURES

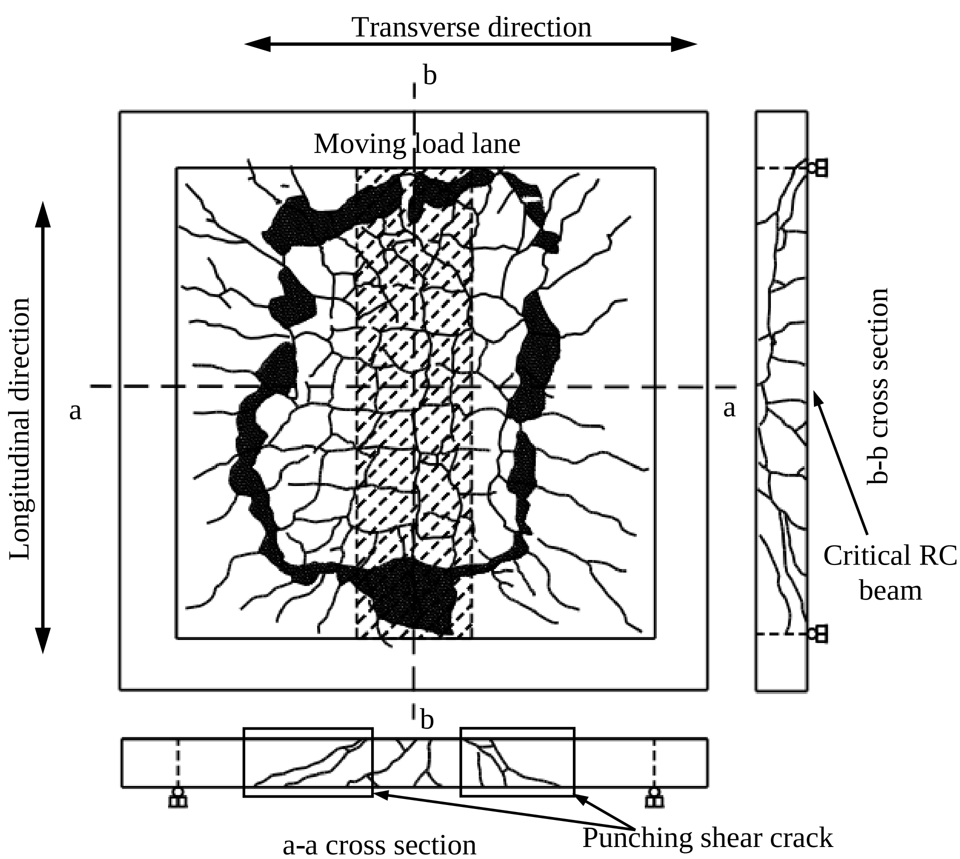

Figure 1 A typical failure crack pattern of an RC slab under cyclic moving loads

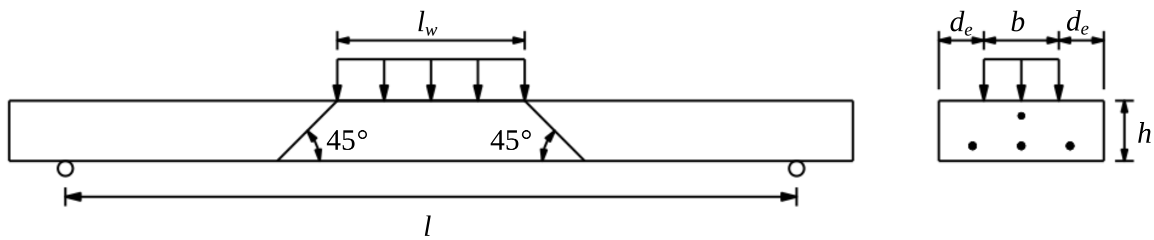

Figure 2 Geometry of the simplified RC beam and the punching shear cracks

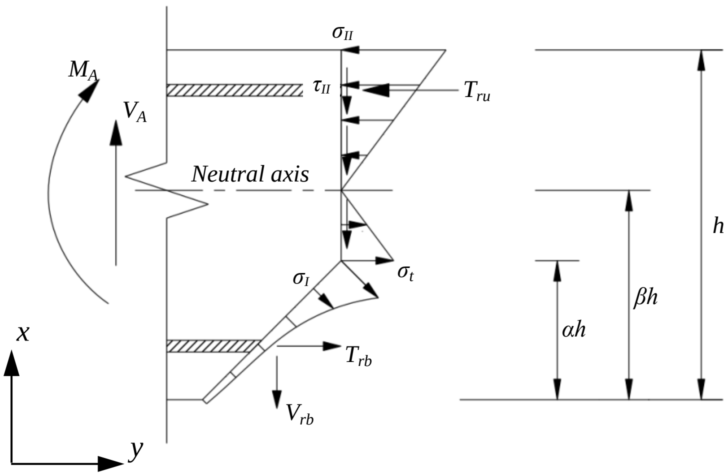

Figure 3 Sectional stresses and forces

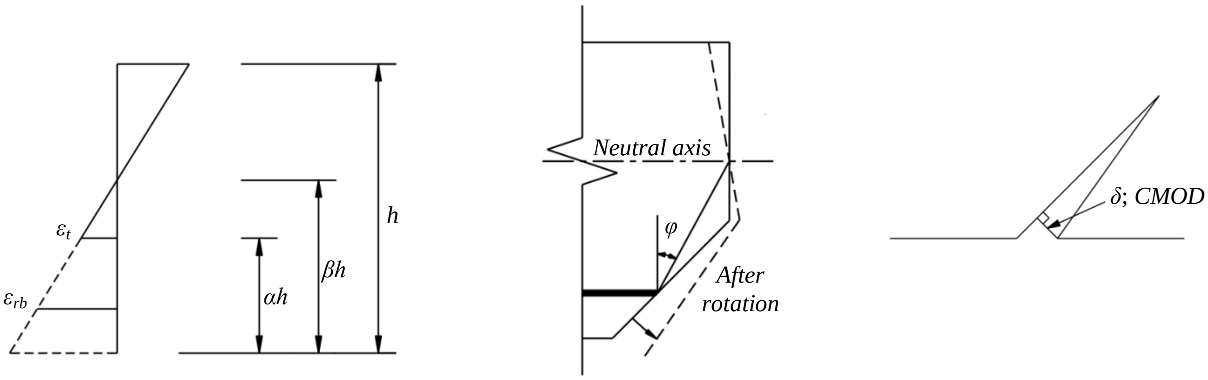

(1) Plane-cross assumption

(2) Section rotating assumption

(3) Linear COD profile assumption

Figure 4 Schematic diagrams for basic assumptions

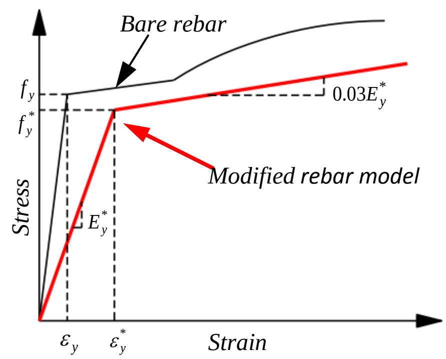

Figure 5 Modified stress-strain relationship for rebars embedded in concrete

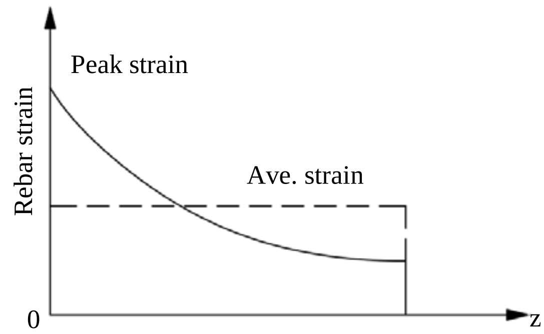

Figure 6 Relation between peak rebar strain and average rebar strain

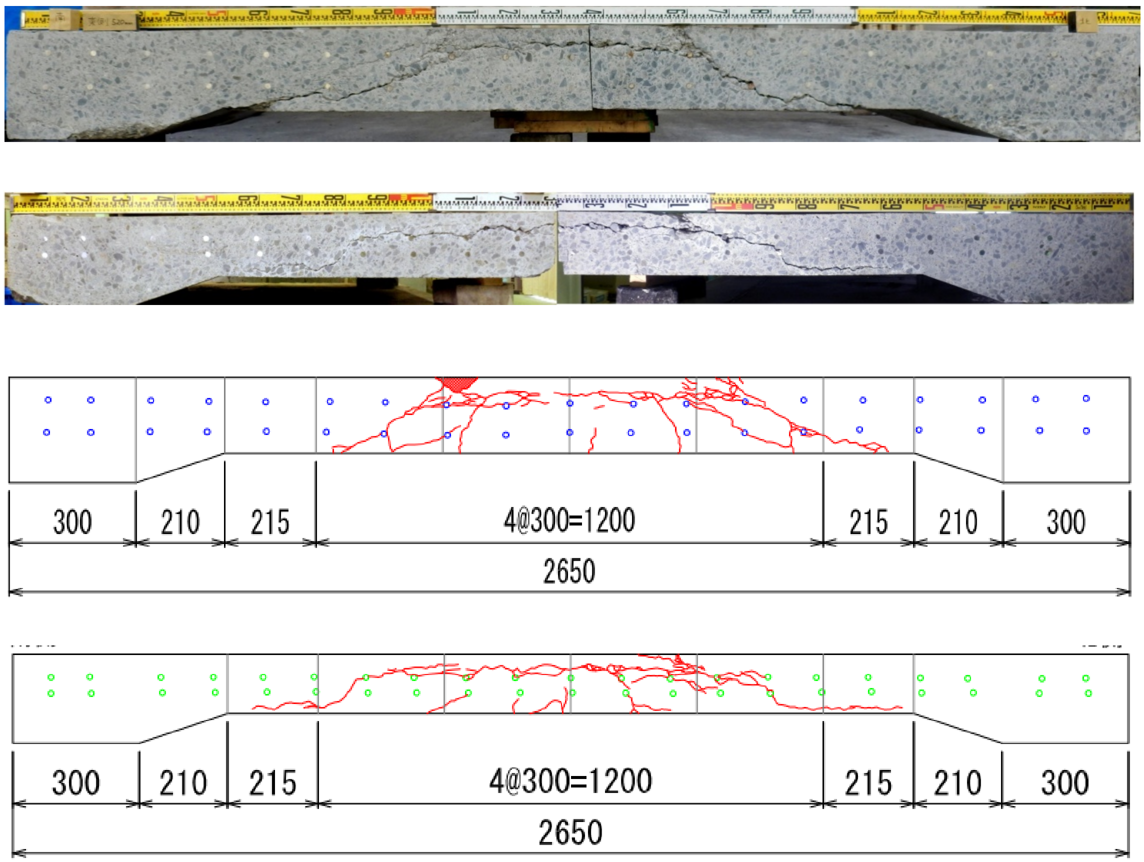

Figure 7 Experimental mid-span crack pattern of several RC slabs provided by Dr. K. Kakuma from CERI

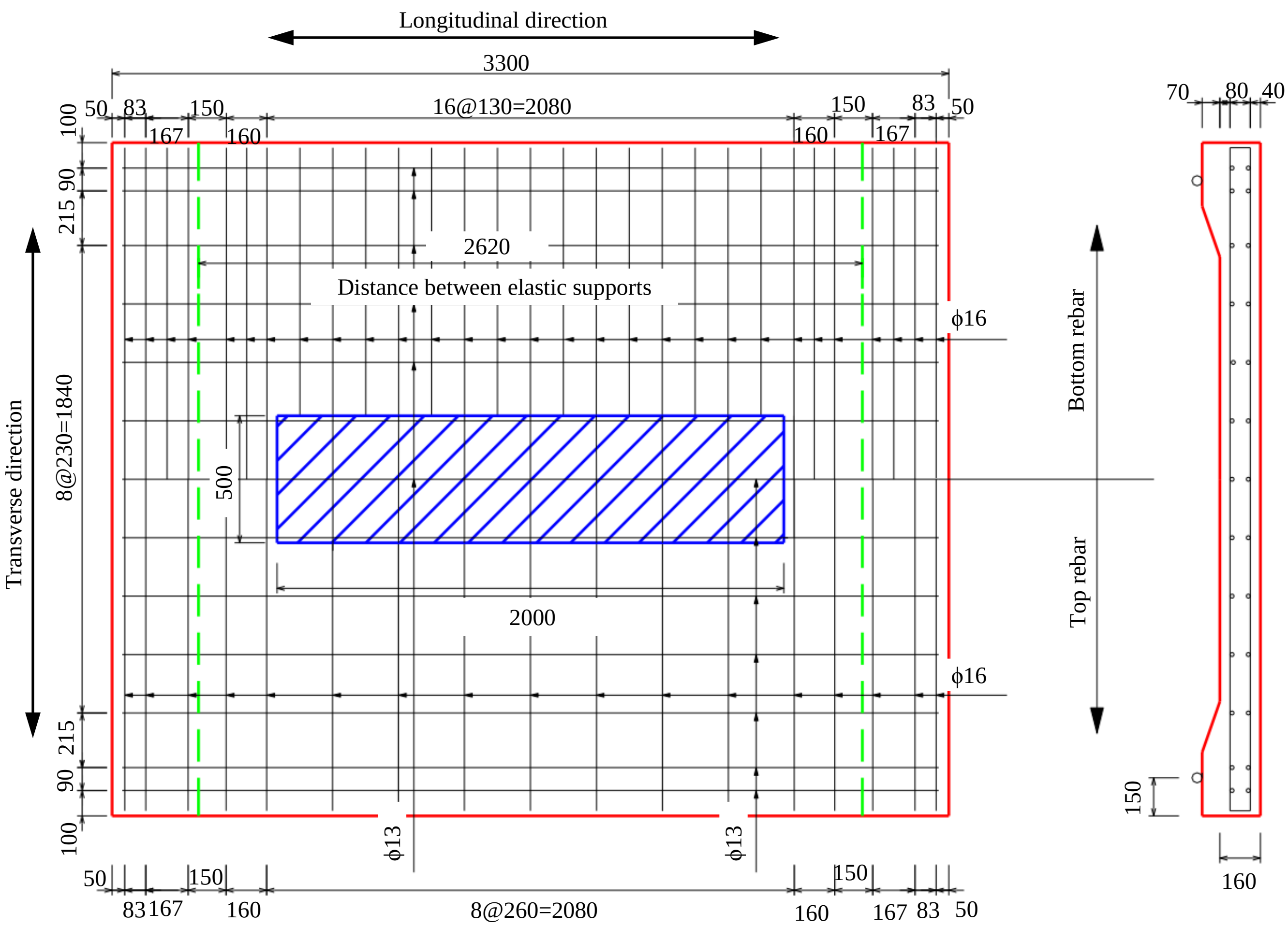

Figure 8 RC slab geometry and reinforcement arrangement [35]

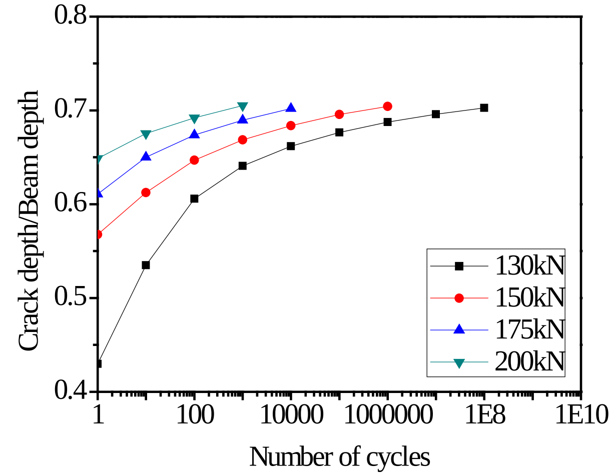

(a) Crack depth/beam depth ratio vs. number of loading cycles

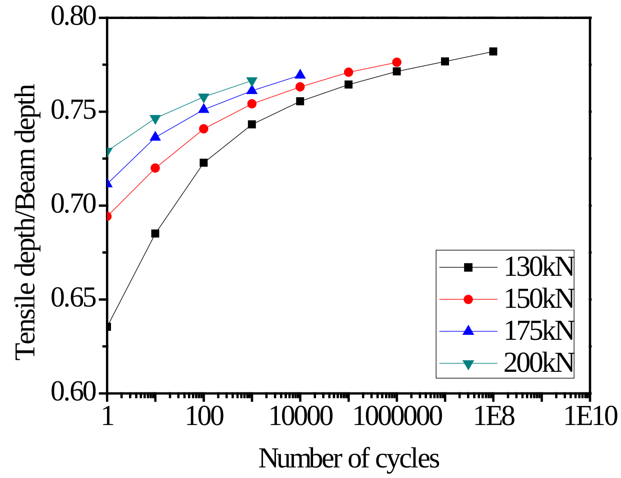

(b) Tensile depth/beam depth ratio vs. number of loading cycles

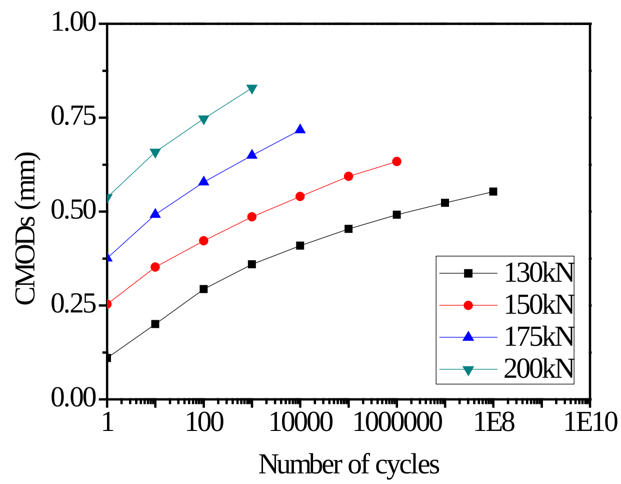

(c) CMODs vs. number of loading cycles

Figure 9 Cracking state parameters vs. number of loading cycles

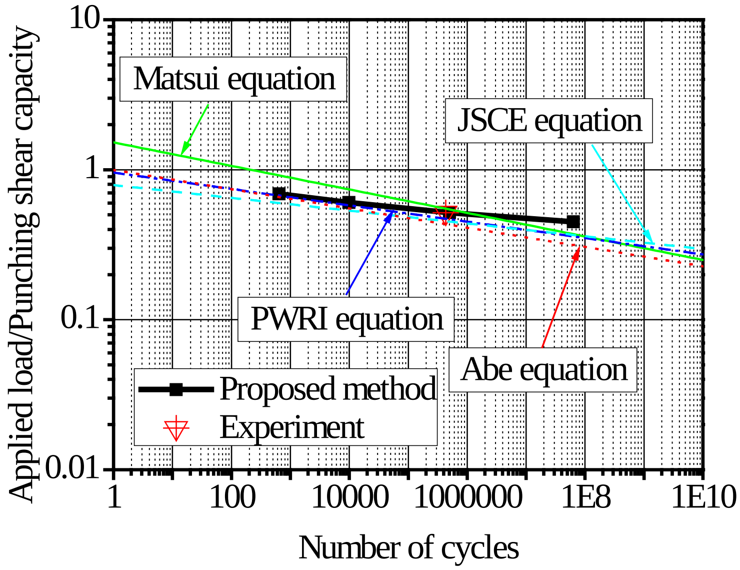

Figure 10 Comparison between fatigue life from different approaches

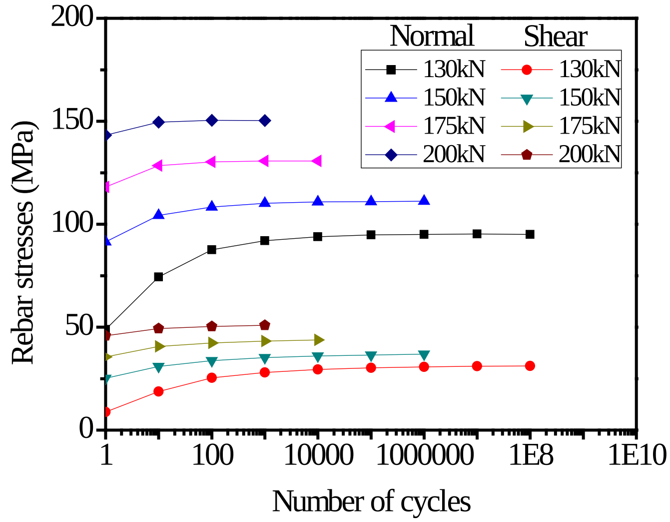

(a) Rebar stresses vs. number of loading cycles

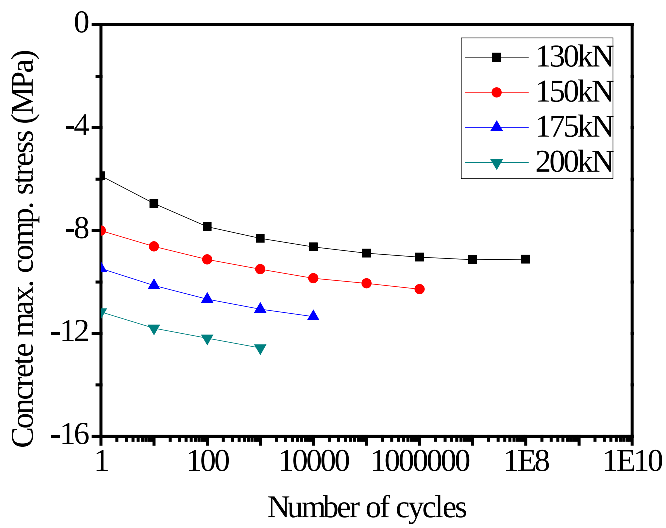

(b) Maximum compression stress of concrete vs. number of loading cycles

Figure 11 Stress evolutions of materials

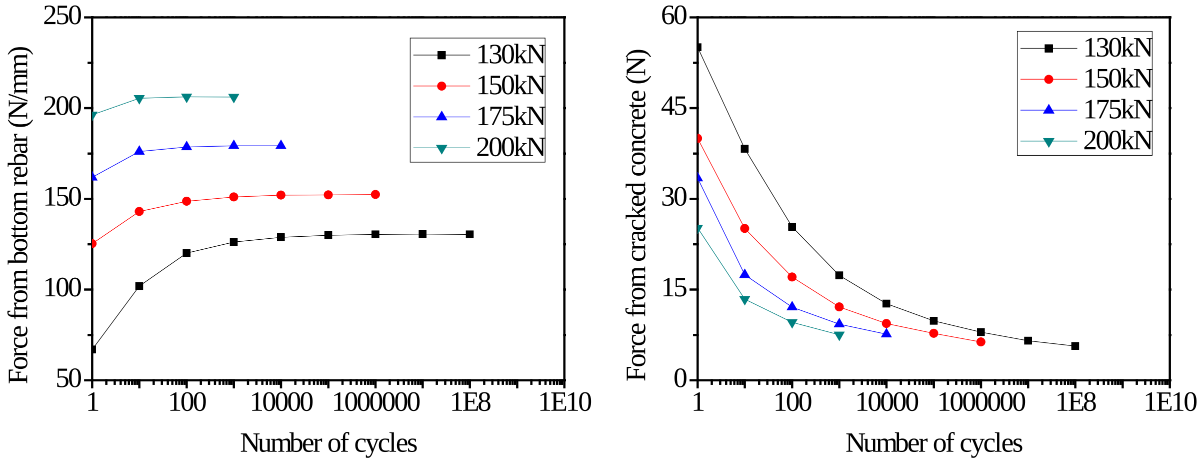

(a) Forces from bottom rebar **(b)** Forces from cracked concrete

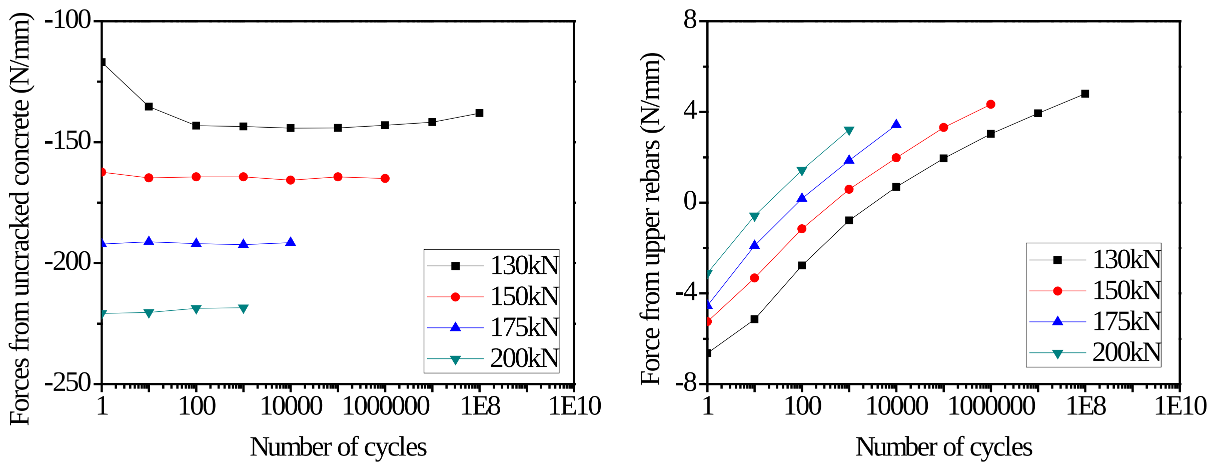

(c) Forces from uncracked concrete **(d)** Force from upper rebars

Figure 12 Forces from different components vs. number of loading cycles for several loading levels

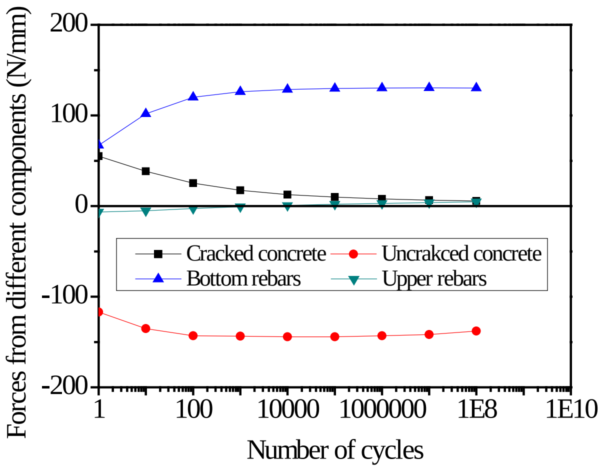

(a) Load=130kN

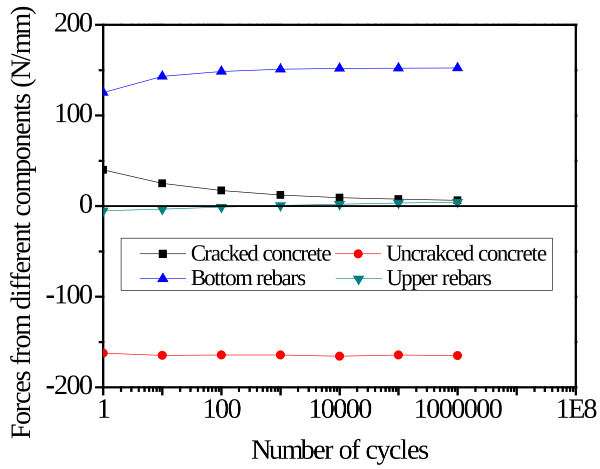

(b) Load=150kN

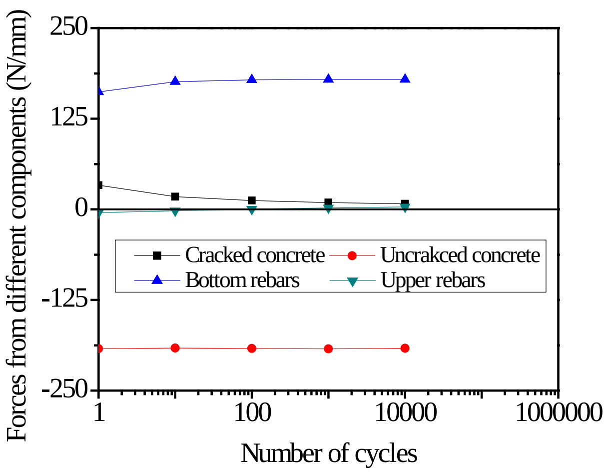

(a) Load=175kN

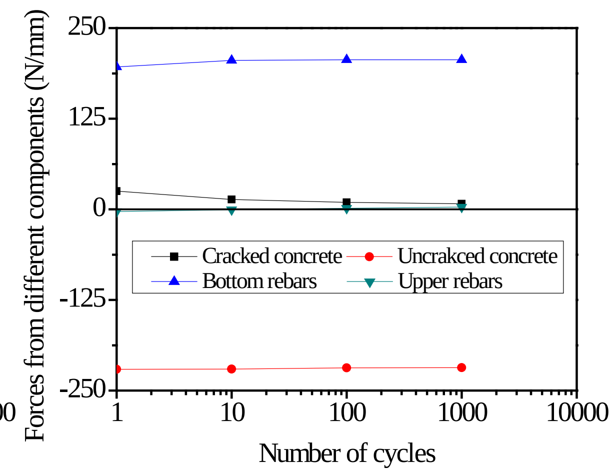

(b) Load=200kN

Figure 13 Comparison of forces from different components vs. number of loading cycles for several loading levels

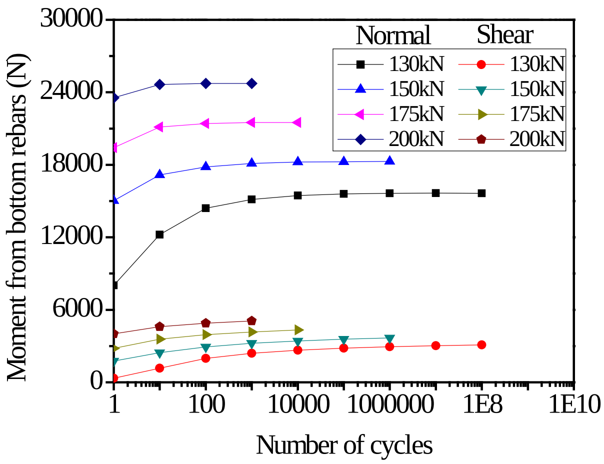

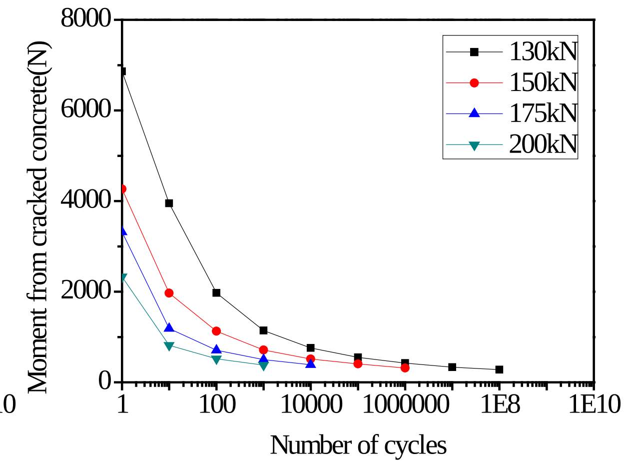

(a) Moment from bottom rebars

(b) Moment from uncracked concrete

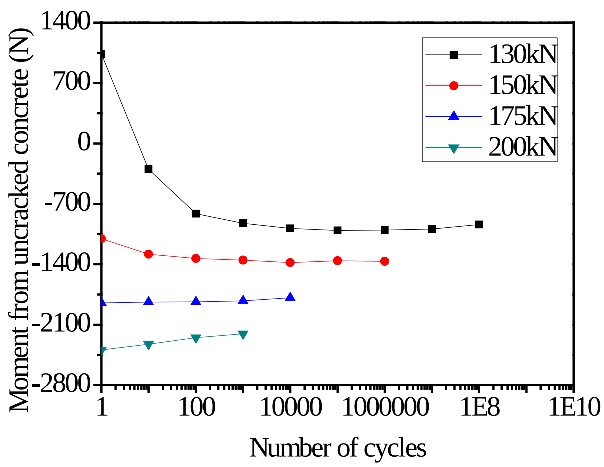

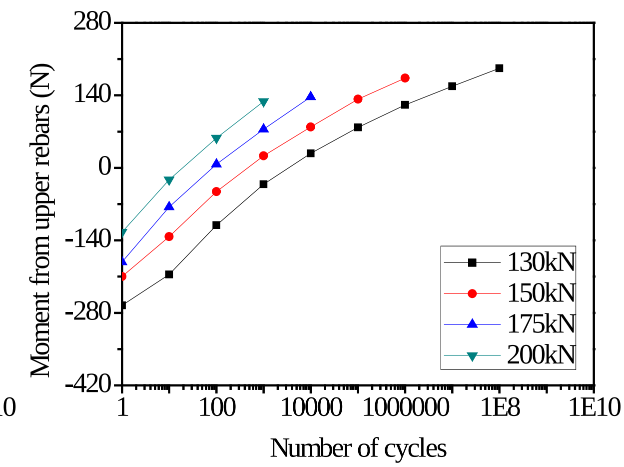

(c) Moment from uncracked concrete

(d) Moment from upper rebars

Figure 14 Moments from different components vs. number of loading cycles for several loading levels

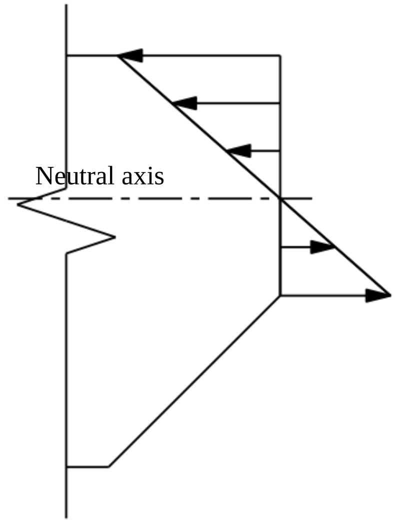

Figure 15 Stress distribution in the uncracked concrete

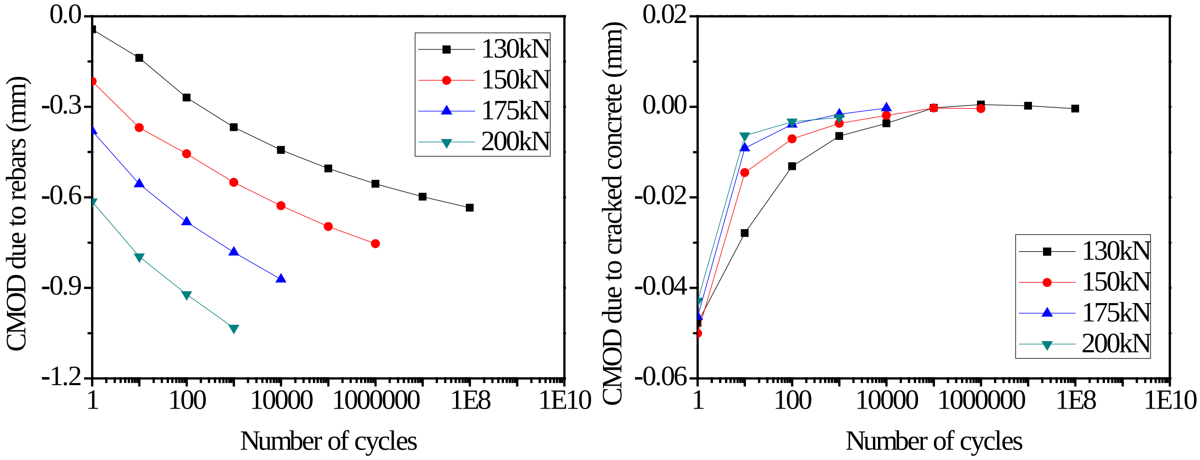

(a) CMODs due to rebar forces **(b)** CMODs due to cracked concrete

Figure 16 CMODs due to different components vs. number of loading cycles for several loading levels